

Synthesis of γ -TiAl by Reactive Spark Plasma Sintering of Cryomilled Ti and Al Powder Blend, Part I: Influence of Processing and Microstructural Evolution

YU SUN, KAUSTUBH KULKARNI, ANIL K. SACHDEV, and ENRIQUE J. LAVERNIA

To provide insight into the influence of an electric field on the kinetics of diffusion, fully lamellar γ -TiAl was processed by a rapid, two-stage, solid-state reactive sintering *via* spark plasma sintering (SPS) of a cryomilled Ti, Al powder blend. Cryomilling was implemented in the current study to attain a nanostructured grain size in the Ti and Al powder blend, and thereby provide insight into the influence of grain size on the underlying diffusion kinetics. Following a two-step process involving SPS at 873 K (600 °C) for 15 minutes and 1523 K (1250 °C) for 30 minutes, a fully lamellar TiAl alloy, with submicron lamellar spacing, was successfully obtained. Microstructural refinement in the Ti and Al powders during cryomilling led to an increase in solid-state diffusion, and the underlying mechanisms are discussed in detail.

DOI: 10.1007/s11661-014-2215-3

© The Minerals, Metals & Materials Society and ASM International 2014

I. INTRODUCTION

SPARK plasma sintering (SPS), a field-assisted sintering technique, has recently been widely applied for the synthesis and consolidation of nanostructured materials.^[1] The densification kinetics of various materials during SPS were significantly enhanced by the concurrently implemented high stress, current density, and heating rate. Studies on the influence of direct current (DC) on diffusivity and reactivity as well as interdiffusion behavior have been reported for various metal-metal (Cu-Ni,^[2] Ni-Ti,^[3] Au-Al,^[4] Ag-Zn^[5]) and metal-metalloid (Nb-C,^[6] Mo-Si,^[7] Ti-C^[8]) systems. In some cases, such as Mo-Si, the reaction products were altered by the presence of a DC field,^[7] whereas in others, for example, Ni-Ti, reactivity was enhanced by the imposition of a DC field, and it was attributed to the changes in defect concentration and mobility.^[3]

TiAl alloys offer high strength, low density, and good corrosion resistance and hence can deliver attractive combinations of good performance and component-weight reduction that are particularly important to the automotive industry.^[9–12] Cost-effective hybrid solid-state processes, involving deformation and reaction, have been developed to prepare γ -TiAl alloys. Acoff and coworkers implemented roll bonding and reaction annealing of elemental Ti and Al foils to fabricate

γ -TiAl sheets with a nearly fully lamellar microstructure.^[13] The application of roll bonding decreased the reactant size, enhanced diffusion by grain refining and defects generation in the constituent foils, and led to a significantly improved reaction kinetics. Recently, combustion syntheses of γ -TiAl from ball-milled^[14] and elemental-blended^[15] Ti and Al powders were implemented by SPS. However, a review of these and other published studies demonstrates that the diffusion mechanisms that govern the reaction synthesis of Ti-Al during SPS remain heretofore poorly understood.

The current study was motivated by two important questions. First, what is the concurrent influence of an electric field and a superimposed pressure on the kinetics of diffusion in the Ti-Al system and what are the conditions that are required for a complete reaction to be attained? Second, can the presence of a nanostructured grain size in the Ti and Al powders significantly enhance diffusion kinetics, and thereby decrease the time and energy required for the reaction to be completed in this system during SPS? To understand these mechanisms, the reactive diffusions of a cryomilled nanostructure Ti and Al powder blend were processed by SPS, and the findings are presented in here in a two-part manuscript. Part 1 (current article) addresses the influence of processing parameters on the powder microstructure and morphology. Part 2 addresses the underlying diffusion mechanisms and the influences of grain size and electric field.

II. EXPERIMENTAL

A. Cryomilling

Commercial-purity Ti (Grade 2) powders (Advanced Specialty Metals, Inc., Nashua, NH) with an average particle size of 80 μm and chemical composition (in wt

YU SUN, Post-Doctoral Researcher, and ENRIQUE J. LAVERNIA, Professor, are with the Department of Chemical Engineering and Materials Science, University of California, Davis, CA 95616. Contact e-mail: yusun@ucdavis.edu. KAUSTUBH KULKARNI, formerly Researcher with the India Science Lab, General Motors Global R&D, Bangalore 560066, India, is now Assistant Professor with the Department of Materials Science and Engineering, Indian Institute of Technology, Kanpur 208016, U.P., India. ANIL K. SACHDEV, Lab Group Manager, is with the Chemical Sciences and Materials Systems Lab, GM Global R&D Center, Warren, MI.

Manuscript submitted July 6, 2013.

Article published online February 19, 2014

pct) of 0.19 pct O, 0.017 pct N, 0.003 pct C, and 0.013 pct Fe, and high-purity Al powders (Valimet, Inc., Stockton, CA) with the average particle size of 25 μm and chemical composition (in wt pct) of <0.01 pct Cu, <0.01 pct Fe, <0.01 pct Mg, <0.01 pct Mn, <0.01 pct Si, <0.01 pct Zn, and <0.05 pct O were blended with a nominal chemical composition of $\text{Ti}_{53}\text{Al}_{47}$ and used as the starting materials for the cryomilling experiments. The cryomilling experiments were performed under liquid argon (L-Ar) [$92 \pm 5 \text{ K}$ ($-181 \pm 5 \text{ }^\circ\text{C}$)] environment using a modified 1-S Szegvari attritor with a stainless steel impeller (rotation speed = 180 rpm) and stainless steel balls (with a diameter of 6.4 mm) for different time intervals (1 to 10 hours). A ball-to-powder ratio of 30:1 was used. 0.4 wt pct stearic Acid ($\text{CH}_3(\text{CH}_2)_{16}\text{CO}_2\text{H}$) was used as a process control agent (PCA) to prevent excessive cold welding of particles to milling media. To prevent atmospheric contamination and to mitigate the hazards associated with the reactivity of Ti, the powders were handled in an inert atmosphere. Additional details of the cryomilling experiments can be found in the published literature.^[16,17]

B. Spark Plasma Sintering

The cryomilled Ti, Al powder blend was consolidated using an SPS-825S DR. SINTER apparatus (SPS Syntex Inc., Japan) under a vacuum condition (~ 6 to 8 Pa), using the following procedure. First, approximately 6 g of powder was loaded into a high-density graphite die with a 20-mm internal diameter. Thin graphite foils were placed between powders and graphite die surfaces to prevent welding and obtain a more uniform current flow. Second, the powders were prepressed in the graphite die under a loading about 100 MPa to obtain a compact form before SPS processing. Third, a sintering pressure of 100 MPa was applied before heating and maintained until the end of sintering. The temperature was measured using a K-type thermocouple positioned in a cavity drilled radially into the graphite die ending 0.5 mm close to the internal diameter of the die. A pulse square waveform with a pattern 12:2 (12 \times 3-ms pulses ON, 6-ms OFF) was used.

A two-step SPS approach was implemented to consolidate the Ti, Al cryomilled powder blend. This procedure was formulated on the basis of a report that the ignition temperature for the exothermic reaction between Ti and Al falls in a range that is close to the melting point of Al.^[18] Hence, complete consumption of Al below the ignition temperature *via* a solid-state reaction with Ti should limit the formation of an inhomogeneous microstructure, as the product phase of this solid-state reaction, TiAl_3 , will react with the balance of Ti and gradually transform to TiAl. Accordingly, the samples were heated from ambient temperature to 823 K (550 $^\circ\text{C}$) at a rate of 100 K/min and then from 823 K to 873 K (550 $^\circ\text{C}$ to 600 $^\circ\text{C}$) at a rate of 25 K/min. After holding at 873 K (600 $^\circ\text{C}$) for 5 to 30 minutes, the samples were heated up to 1473 K (1200 $^\circ\text{C}$) at a rate of 100 K/min and then from 1473 K to 1523 K (1200 $^\circ\text{C}$ to 1250 $^\circ\text{C}$) at a rate of 25 K/min, and held at 1523 K (1250 $^\circ\text{C}$) for 1 to 30 minutes. After

completion of the sintering step, the samples were allowed to cool down to ambient temperature. The samples had the dimension of $\Phi 20 \times 5 \text{ mm}$.

C. Characterization

The cryomilled powders, SPS-processed TiAl specimens, were characterized using X-ray diffraction (XRD), scanning electron microscopy (SEM), and transmission electron microscopy (TEM). The XRD studies were carried out in a Scintag XDS 2000 X-ray diffractometer using $\text{Cu } K_\alpha$ radiation. The SEM was performed in an FEI XL-30 FEG scanning electron microscope. A Philips CM12 microscope operating at 120 kV was utilized for TEM observations. The powder TEM samples were prepared by embedding the powders in Gatan G-1 epoxy, followed by mechanical polishing dimpling, and ion milling using a Gatan 691 precision ion polishing system.

III. RESULTS

A. Cryomilling Behavior of Ti, Al Powder Blend

The chemical compositions of the as-received and 10-hour-cryomilled powder blends were analyzed by Lu-vak, Inc., and the amounts of C, O, N, H and Fe impurities are shown in Table I.

The results showed an increase in the amount for all impurity elements, as anticipated from the atmospheric contamination that occurs during milling and the use of stearic acid as PCA. The powder morphology was characterized using SEM, and the back-scattered electron (BSE) images are shown in Figures 1(a) through (h). For the as-received powders, as shown in Figures 1(a) and (b), both Ti (bright) and Al (dark) particles are spherical with the average sizes of approximately 80 and 25 μm , respectively. Following a 2-hour-cryo milling experiment, most of the Ti particles remain spherical although several of them were axially deformed, and no cold welding between Ti particles was evident (see Figures 2(c) through (d)). Al particles were cold welded and agglomerated into clusters, and some of them were also cold welded to Ti particles. An increase in milling time to 6 hours, Figures 1(e) and (f), led to a significant reduction in the Al particle size and in the greater deformation of the Ti particles. Cold welding can be observed between Ti and Al or between Al and Al, but Ti particles were not fragmented, and failed to reveal any evidence of cold welding between themselves. Increasing the milling time to 10 hours failed to promote the fragmentation of the Ti particles, although deformation increased as shown in Figures 1(g) and (h).

The cryomilled and as-received powders were analyzed *via* XRD, and the associated diffraction patterns are shown in Figure 2. The diffraction patterns failed to show any additional diffraction peaks, other than those corresponding to pure Ti and Al. The Ti and Al peaks are significantly reduced in intensity and broadened after cryomilling for 2 hours. Increasing the cryomilling time from 2 to 10 hours led to a slight increase in the

Table I. The Amounts of C, O, N, H and Fe Impurities Present in As-Received and 10-h-Cryomilled Ti, Al Powder Blend

Powder	C (wt pct)	O (wt pct)	N (wt pct)	H (wt pct)	Fe (wt pct)
As-received	0.006	0.23	0.056	0.041	0.02
Cryomilled	0.05	1.16	0.77	0.052	0.078

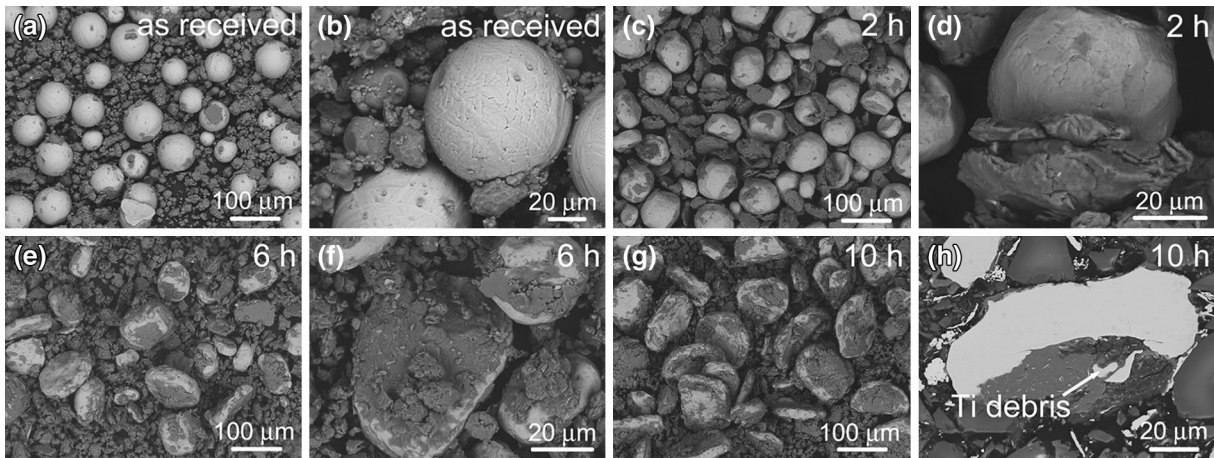


Fig. 1—SEM images of as-received (a, b) and 2-h (c, d)-, 6-h (e, f)-, and 10-h (g, h)-cryomilled Ti, Al powder blends.

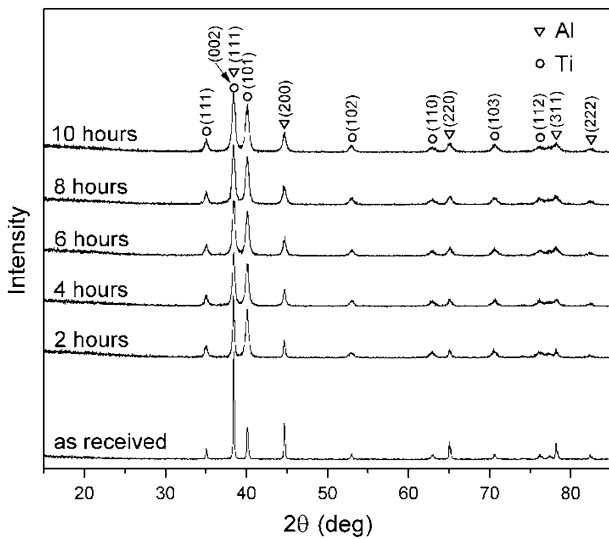


Fig. 2—XRD patterns of as received and 2-, 4-, 6-, 8-, 10-h-cryomilled Ti, Al powder blends.

broadening of the peaks with no significant changes being observed in their corresponding intensities. The dislocation density ρ can be estimated by the follow equation^[19]:

$$\rho = \frac{2\sqrt{3}\varepsilon}{D \times b}, \quad [1]$$

where ε is the lattice microstrain, D is the crystallite diameter, which corresponds to the dimension of coherent diffraction domains including dislocation cells and subgrains,^[20] and b is the burger's vector. ε and D can be

Table II. The Estimated Dislocation Densities in Ti and Al of the As-Received and of the Cryomilled Powders

Powder	ρ_{Ti} (m ⁻²)	ρ_{Al} (m ⁻²)
As-received	3.4×10^{14}	5.9×10^{13}
2 h cryomilled	2.2×10^{15}	2.9×10^{14}
4 h cryomilled	2.3×10^{15}	1.4×10^{15}
6 h cryomilled	3.1×10^{15}	2.3×10^{15}
8 h cryomilled	2.9×10^{15}	2.7×10^{15}
10 h cryomilled	2.7×10^{15}	2.5×10^{15}

measured from XRD data, and the estimated dislocation densities in Ti and Al of the as-received and the cryomilled powders are listed in Table II.

To provide insight into the evolution of grain size during cryomilling, the 2 to 10-hour cryomilled powder blends were analyzed by TEM, and the average grain sizes for Al and Ti were statistically determined by measuring 300 individual grains for each data. Figures 3(a) through (f) show the bright-field and the corresponding dark-field TEM images for Al in the powder blends for different cryomilling times. Al grains with sizes smaller than 100 nm as well as grains with sizes of about several hundred nanometers can be observed after 2 hours of cryomilling. Increasing the milling time to 4 hours led to a significant reduction of the Al grain size. However, further increasing the milling time to 10 hours did not lead to a significant grain refinement. The average grain size is summarized and shown in graphic form in Figure 4. The results show that after 2 hours of cryomilling, Al has an average grain size of 108 nm. The rate of grain size reduction during

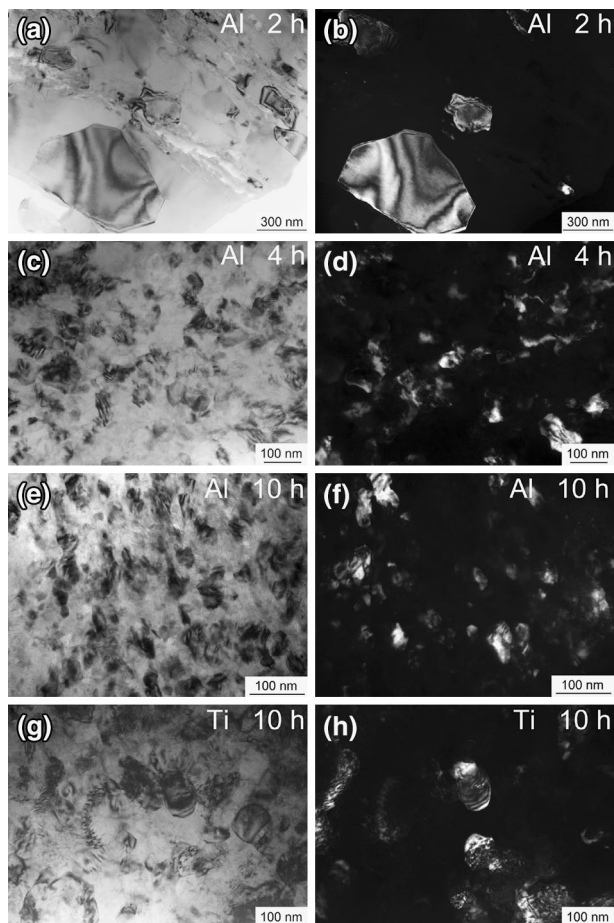


Fig. 3—Bright field and dark field TEM images for Al in 2-h (a, b)-, 4-h (c, d)-, 10-h (e, f)-cryomilled powder blends and Ti in 10-h (g, h) cryomilled powder blends.

cryomilling decreases after 4 hours, and the grain size for Al is reduced from 65 to 42 nm after 10 hours. Figures 3(g) and (h) show the TEM images for Ti in the 10-hour-cryomilled powder blend. The grains shown in the image reveal a multimodal grain size distribution, with some grains larger than 100 nm whereas others are smaller than 50 nm. The average grain sizes were also determined for the Ti powder and are summarized in Figure 4, as a function of milling time. As in the case with Al, the rate of Ti grain size refinement levels off after 4 hours and attains a value of 100 nm after 10 hours of cryomilling.

B. SPS of Cryomilled Ti, Al Powder Blend

The cryomilled powder blends were subjected to solid-state reactive sintering by SPS. Since Al has a relatively lower melting point of about 933 K (660 °C), we designed a two-stage sintering cycle. First, the cryomilled Ti and Al powder blend is consolidated by SPS at 873 K (600 °C), and second, a reactive consolidation step is carried out at a higher temperature, typically 1523 K (1250 °C), to reach the desired $Ti_{53}Al_{47}$ alloy designated by a mark on the Ti-Al phase diagram^[21]

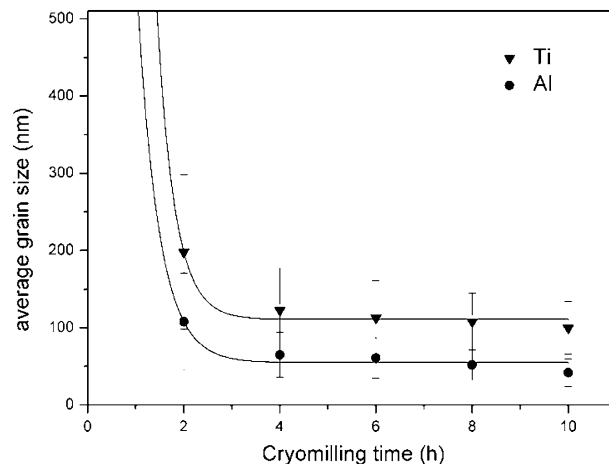


Fig. 4—Average grain sizes for Ti and Al in the powder blends cryomilled for 2 to 10 h.

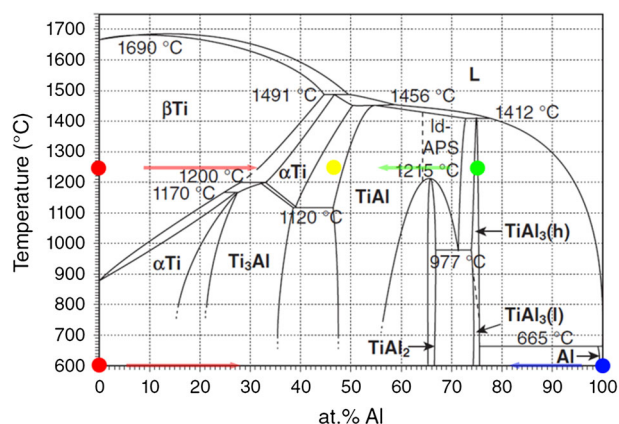


Fig. 5—Ti-Al binary phase diagram.^[21]

(Figure 5). The selection of the latter temperature was prompted by evidence that the alloy is located in the $\alpha + \gamma$ region at 1523 K (1250 °C) and the $\alpha + \gamma \rightarrow \alpha_2 + \gamma$ transformation during the cooling process is essential for the formation of lamellar microstructure. Moreover, processing at 1523 K (1250 °C) is adequate enough for the formation of TiAl, densification, and homogenization to occur in a reasonable time.

In order to establish the amount of time required to reactively consume the entire Al during SPS at 873 K (600 °C), we completed a series of SPS experiments for times of up to 30 minutes, and analyzed the resultant samples *via* SEM and XRD. The associated backscattered SEM images and XRD patterns are shown in Figures 6 and 7, respectively. After 5 minutes, a layer of a new phase is evident between Ti and Al, and this phase was identified as $TiAl_3$ on the basis of the XRD patterns, consistent with the published results.^[13,22,23] The presence of voids was evident along phase boundaries (see Figure 6(b)) which is attributed to the difference in the Ti and Al diffusivities (*i.e.*, to Kirkendall porosity) and to the changes in volumes during the reaction.^[24] It is unlikely that they are associated with the formation of TiN during cryomilling since the

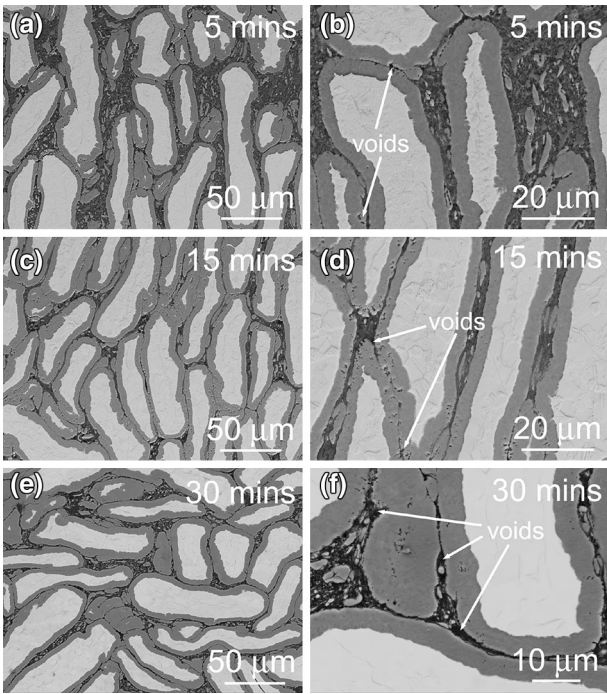


Fig. 6—Back backscattered SEM images for the consolidated cryomilled Ti, Al powder blend samples which were SPS'ed at 873 K (600 °C) for 5 (*a, b*), 15 (*c, d*), and 30 (*e, f*) min.

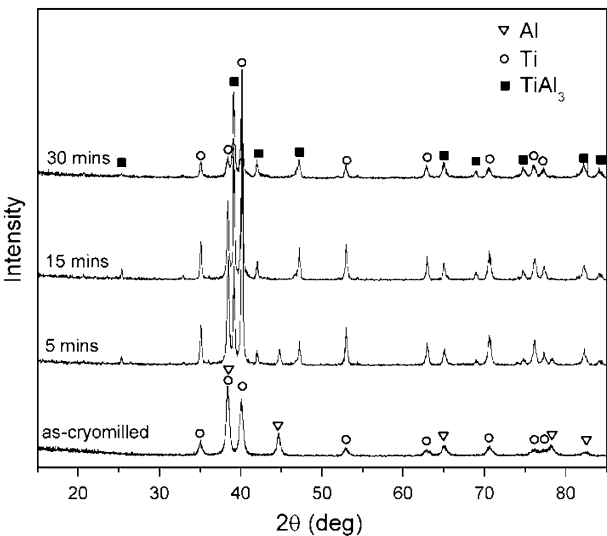


Fig. 7—XRD patterns for the as-cryomilled Ti, Al powder blend and its consolidated samples which were SPS'ed at 873 K (600 °C) for 5, 15, and 30 min.

formed oxides and nitrides during cryomilling are suggested to have a size about 4 nm based on the data from the three-dimensional atom probe analyses according to a recent study.^[25] After SPS for 15 minutes, the diffusion layer was fully developed with a concomitant increase in the concentration of voids, as shown in Figures 6(c) and (d). The comparison of the XRD patterns from the samples, SPS-ed for 5 and 15 minutes, shows that the diffraction peaks corresponding to Al

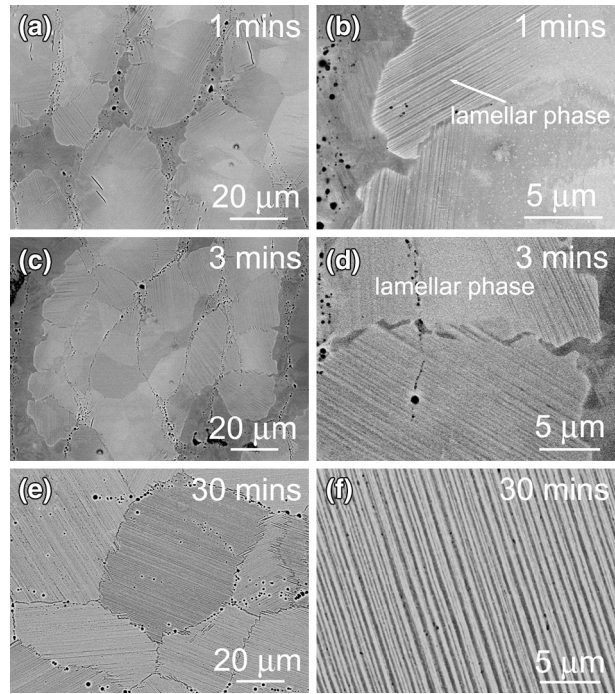


Fig. 8—Back backscattered SEM images for the consolidated cryomilled Ti, Al powder blend subjected to two-stage reactive sintering that SPS at 873 K (600 °C) for 15 min and then 1523 K (1250 °C) for 1 (*a, b*), 3 (*c, d*), and 30 (*e, f*) min.

(200) vanish after 15 minutes. In the case of the sample SPS-ed for 5 minutes, the Ti (002) and Al (111) peaks overlap. The comparison of the peak at ~38.5 deg to the peak corresponding to Ti (102) from the XRD pattern of the sample, SPS-ed for 15 minutes, shows that they had the same intensity ratio as did the corresponding diffraction peaks on the standard XRD diffraction pattern for Ti (PDF#44-1294). This result suggests that almost the entire Al was consumed after SPS at 873 K (600 °C) for 15 minutes. Increasing the SPS time from 15 to 30 minutes did not change the types of constituent phases present, which were Ti and TiAl₃.

The aforementioned two-stage sintering methodology was applied to cryomilled Ti, Al powder blends; that is, SPS at 873 K (600 °C) for 15 minutes followed 1523 K (1250 °C) for up to 30 minutes. The corresponding BSE images and XRD patterns are shown in Figures 8 and 9, respectively. The XRD results show that the constituent phases are TiAl and Ti₃Al for all of the three samples SPS-ed at 1523 K (1250 °C) for 1, 3, and 30 minutes. Moreover, no pure Ti or TiAl₃ is seen even after only 1-minute sintering at 1523 K (1250 °C). SEM analyses reveal several interesting features like a high Al concentration region and a lamellar phase precipitated along the boundary of these areas in the sample SPS-ed for 1 minute, as shown in Figures 8(a) and (b). The growth of lamellar phase increased with the increasing SPS time, and a significant increase in the amount of the lamellar phase can be observed along the high Al content area after 3 minutes (see Figure 8(d)). Moreover, a fully lamellar microstructure can be observed after SPS at 1523 K (1250 °C) for 30 minutes. The lamellar colonies have a fine $\gamma + \alpha_2$ microstructure with submicron

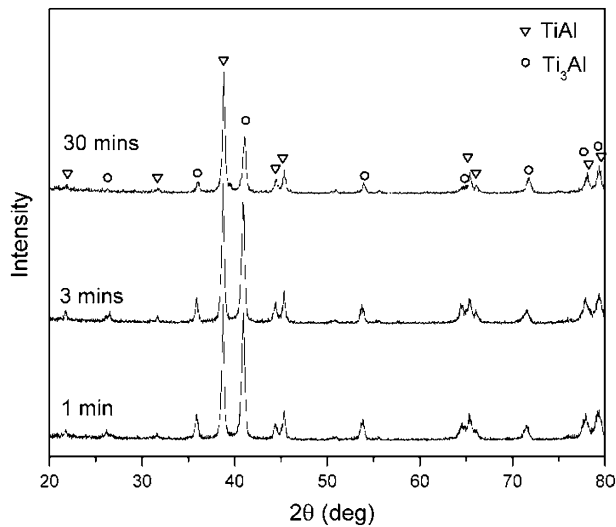


Fig. 9—XRD patterns for the consolidated cryomilled Ti, Al powder blend subjected to two-stage reactive sintering that SPS at 873 K (600 °C) for 15 min and then 1523 K (1250 °C) for 1, 3, and 30 min.

lamellar spacing, as shown in Figure 8(f). All the samples are not fully dense as the pores can be found along the area which developed from the particle boundaries as shown in Figure 6. The final density is about 96.5 pct for the sample which was consolidated at 873 K (600 °C) for 15 minutes and 1523 K (1250 °C) for 30 minutes.

IV. DISCUSSION

To provide insight into the mechanisms that govern the reaction kinetics in the cryomilled Ti-Al powder blends, it is appropriate to first discuss here the origin of the structural refinement during cryomilling, paying particular attention to the influence of cryomilling parameters on the resultant powder morphology and microstructure. A discussion of the diffusive reaction kinetics is included in the part 2 of this paper.

A. Particle Evolution of Ti, Al Powder Blend During Cryomilling

Cryomilling has been widely used to refine the grains of pure metal or ductile alloy powders.^[17,26] However, cryomilling involving two different ductile components has heretofore never been reported. The particle morphology usually evolves from being flat and angular during the initial stages of cryomilling into an equiaxed morphology with increasing milling time. In a mechanistic study of mechanical alloying involving two different ductile components, it was suggested that the ductile components get flattened by a microforging process at an early stage and then cold welded to each other and form a lamellar structure of the constituent metals. With further milling, the cold-welded particles are work hardened and fragmented into equiaxed dimensions with a retained fine lamellar structure.^[27]

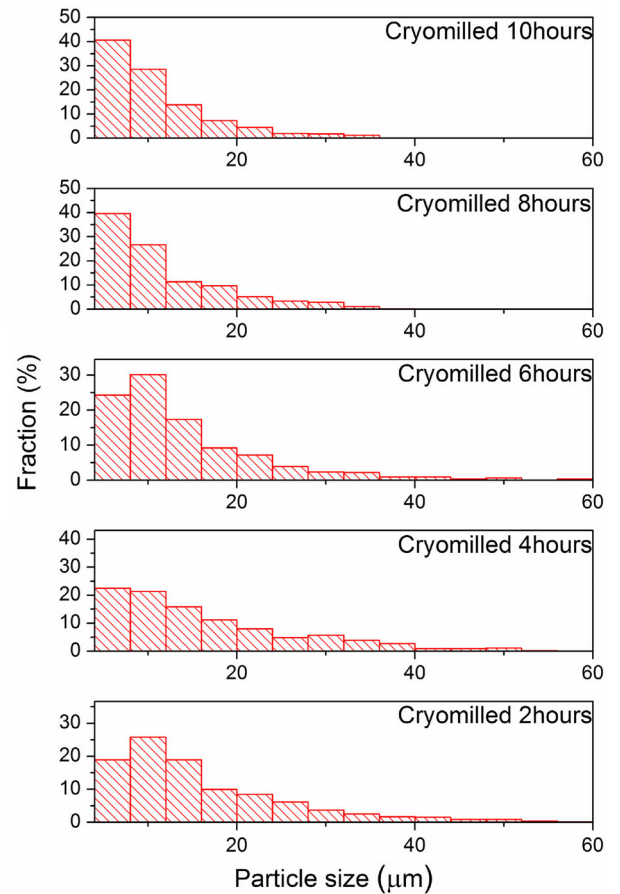


Fig. 10—Histograms of the Al particle size distribution in 2 to 10 h cryomilled powders.

In our study, the observed differences in morphology between the Ti and Al particles in the cryomilled powder blend suggest that different deformation mechanisms govern the two constituents. The Ti particles exhibited limited deformation even after 10 hours of cryomilling, and their morphology remained similar to individual (pure Ti not blended with Al) Ti particles milled for 1 to 2 hours.^[28] Examination of the cross section of cryomilled Ti particles, as shown in Figure 1(f), failed to reveal any signs of fragmentation although small amounts of Ti debris was occasionally seen embedded in Al particles, as shown in Figure 1(h) denoted by an arrow. However, the flattened and elongated shape of Ti after cryomilling allow an easier diffusion during SPS processing by reducing the diffusion length in the transverse direction of the particles. The Al particles have been significantly refined after cryomilling with times up to 10 hours, as illustrated in Figure 10, which shows the particle size distribution of Al for different cryomilling times. The starting 325 mesh Al powders have a normal size distribution between 5 and 100 μm. After cryomilling for 2 hours, the particle size is increased because of cold welding and agglomeration. After 4 hours, there is a slight decrease in the proportion of ~12 μm particles and an increase in the proportion of 30 to 40 μm particles, consistent with the agglomeration of Al powders. The proportion of particles smaller than 12 μm significantly

increases after cryomilling for 6 hours, and the proportion of particles smaller than 8 μm significantly increase after cryomilling for 8 hours consistent with the fracture of a heavily cold worked structure.^[29]

B. Microstructural Evolution of Ti and Al During Cryomilling

The microstructural refinement process during cryomilling involves the generation of dislocations, the formation of subboundaries and the formation of high-angle grain boundaries, which transform from low angle subboundaries.^[17] Grain refinement of Al (FCC) occurs relatively homogeneously through the formation of dislocation cells or subgrains aligned into different shear planes, then these dislocation cells or subgrains gradually evolve into arrays of ultrafine grains separated by high-angle boundaries.^[26] In the case of HCP metals, such as Ti, new grains nucleate along the initial grain boundaries because of the high stress required to activate multiple slip systems. The internal defect microstructure of the cryomilled powders critically influences diffusion kinetics. In our study, Ti and Al in the cryomilled powder blend showed different degrees of grain size refinement and increase in dislocation density. For the 10-hour-cryomilled powder blend, the Al and Ti had average grain sizes of 42 and 100 nm, respectively. Moreover, the increases in dislocation density for Ti and Al were 8 times and 40 times, respectively, after 10-hour-cryo milling. Their average grain sizes are larger than that of individually cryomilled Ti- or Al- based on literature reports,^[30,31] especially for Ti which reportedly can attain an average grain size of 20 nm after 8-hour-cryomilling. The driving force of this grain refinement is the strain energy received from impact with the balls driven by the impeller's kinetic energy. Macroscopically, the impeller's kinetic energy is transferred to the Ti and Al in the powder blend during cryomilling, and the final microstructure will be affected by the strain energy introduced during milling.^[32]

Recently, a mathematical framework was formulated by Lin *et al.*^[33] and used to investigate the magnitude of strain energy introduced to the powders during attritor ball milling. The strain energy introduced to the powders per unit mass was considered to evolve as contributions from the normal and shear strain components that occur during individual collisions, and can be estimated on the basis of the following equation^[33]:

$$U_i = fT(U_{E\sigma_z} + U_{E\sigma_r} + U_s)/m, \quad [2]$$

where U_i is the strain energy per unit mass, f is the collision frequency, T is the milling time, and m is the mass of powders. The strain energy introduced by axial normal strain ($U_{E\sigma_z}$), the radius normal strain ($U_{E\sigma_r}$) and the shear strain (U_s) can be calculated using the following equations,^[33] respectively.

$$U_{E\sigma_z} = 2\pi \Delta h Y \left\{ -\frac{h}{2\mu} r_E - \left(\frac{h}{2\mu}\right)^2 + \left(\frac{h}{2\mu}\right)^2 \exp\left(\frac{2\mu}{h} r_E\right) \right\} \quad [3]$$

$$U_{E\sigma_r} = 2\pi \Delta h Y \left(\sqrt{\frac{h}{h - \Delta h}} - 1 \right) \left\{ -\frac{h}{2\mu} r_E - \left(\frac{h}{2\mu}\right)^2 + \left(\frac{h}{2\mu}\right)^2 \exp\left(\frac{2\mu}{h} r_E\right) - \frac{r_E^2}{2} \right\} \quad [4]$$

$$U_s = K(\pi r_E^2 h) \left[\frac{1}{n+1} r_{zx}^{n+1} + \frac{1}{n+1} r_{zy}^{n+1} \right] \quad [5]$$

In this model, the powders that are trapped between the milling media were assumed to have a cylindrical geometry with a radius of r_E and a height of h , which can be evaluated as^[33]

$$r_E = 0.9731 \overline{\overline{v_B}}^{0.4} (\rho_B/E_B)^{0.2} r_B \quad [6]$$

$$h = 0.8 r_B \rho_B / 3 \rho_P C, \quad [7]$$

where $\overline{\overline{v_B}}$ is the average value of the normal component of the velocity difference with respect to angles. It can be calculated by the follow equation^[33]:

$$\overline{\overline{v_B}} = FR \quad [8]$$

F is the impeller's rotational frequency, R is the radius of the milling vessel, r_B , ρ_B and E_B are the radius, the density, and the Young's modulus of balls, respectively, ρ_P is the powder density, and C is the ball-to-powder mass ratio. The experimental parameters and physical constants for attritor, milling ball, and powders are listed in Table III.^[34,35] The calculated $U_{E\sigma_z}$, $U_{E\sigma_r}$, U_s and U_i are listed in Table IV. These results suggest that the strain energy experienced by Al in the 10-hour-cryomilling experiment is almost twice as much as that corresponding to Ti. In related studies, Koch^[32,36] reported the mill energy can influence the values of the minimum grain size attained by ball milling, as well as the kinetics of the process, and that higher energy milling will lead to smaller minimum grain size and faster grain refinement kinetics. The milling energy calculations in our study are consistent with the measured grain size refinement and the decrease in dislocation density increase following cryomilling.

C. Evolution of Microstructure During SPS

In our study, the diffusive reactions during SPS proceeded in sequence as shown by the arrows marked in Figure 5; Reaction 1 ($\alpha\text{Ti} + 3\text{Al} = \text{TiAl}_3$) at 873 K (600 °C) is followed by Reaction 2 ($2\text{Ti} + \text{TiAl}_3 = 3\text{TiAl}$) at 1523 K (1250 °C). In the related study, Voisin *et al.*^[37] studied the temperature distribution of a TiAl alloy sample during SPS and demonstrated that there is a correction factor that is required to account for the difference between the measured and the actual sample temperatures, and that the magnitude of this factor is facility dependent. We reached a similar conclusion in our study based on the temperature measurements as reported in Part II of our manuscript. In our SPS experiments, all the Al reacted with Ti during the first step at

Table III. Experimental Parameters and Physical Constants for Attritor, Milling Ball, and Powders^[34]

Constants	Al	Ti
Density ρ_p (kg/m ²)	2700	4507
Ultimate tensile yield strength Y (MPa)	225	325
Shear work-hardening factor K (MPa)	175	315
Shear work-hardening index n	0.2	0.18
Ball/powder fraction coefficient μ	0.47	0.49
Ball-to-powder mass ratio C	30	15
713 K (440 °C) stainless ball radius r_B (m): 3.175×10^{-3}		
713 K (440 °C) stainless ball density ρ_B (kg/m ²): 7650		
713 K (440 °C) stainless ball Young's modulus E_B (GPa): 200		
Total mass of balls M (kg): 30		
Total milling time T (h): 10		
Impeller's rotational frequency F (round/s): 3		
Radius of the milling vessel R (m): 0.13		

Table IV. Calculated Strain energy (U_i) and the component introduced by axial normal strain ($U_{E\sigma_z}$), radius normal strain ($U_{E\sigma_r}$) and shear strain (U_s)

	$U_{E\sigma_z}$ (J)	$U_{E\sigma_r}$ (J)	U_s (J)	U_i (J/g)
Ti powder	828×10^{-5}	383×10^{-5}	251×10^{-5}	5.52×10^6
Al powder	790×10^{-5}	459×10^{-5}	137×10^{-5}	10.49×10^6

950 K (677 °C) (sample's actual temperature) to form TiAl₃.^[38] A small amount of TiAl₃ likely formed before the sample reached the melting point of Al at 933 K (660 °C), and this was demonstrated in part 2 of this manuscript. At this stage, most of the Al would have been encapsulated by the Ti particles and the newly formed TiAl₃ by the time the graphite reached 950 K (677 °C). Hence, the free surface available for Al evaporation is likely to have originated in the perimeter of the die, where the gap formed at the inner surface of die is in direct contact with the atmosphere. Accordingly, if one takes into account the 0.1-mm plunger dimensional tolerance, the maximum area for possible evaporation of Al is 0.0398 cm². The maximum molar evaporation flux (J_{\max}) can be estimated using the Hertz-Knudsen equation^[39]:

$$J_{\max} = \frac{P_v}{\sqrt{2\pi MRT}} \quad [9]$$

M is the molecular weight, R is the universal gas constant, and T is the temperature at evaporating surface. P_v is the standard vapor pressure, and which for the melted Al is given by Reference 34,

$$\log P_v \text{ (Pa)} = 10.917 - 15630/T \quad [10]$$

At 950 K (677 °C), $P_v = 2.91 \times 10^{-6}$ Pa, and $J_{\max} = 6.78 \times 10^{-8}$ g cm⁻² s⁻¹. Since all the Al reacted with Ti in 15 minutes, then the maximum amount of Al evaporation is 2.42×10^{-4} g. If one compares this value to the Al content in each sample (approximately 2 g), the maximum loss of Al due to evaporation is about 0.012 wt pct. This analysis confirms that the loss of Al in our experiments can be neglected, and hence, it does not

affect the reaction mechanism related to Al diffusion through TiAl₃.

In our experiments, the reaction sequence is consistent with the published studies in which Ti and Al solid-state reactions occur under normal annealing,^[13,40] and no formation of other intermediate phases such as TiAl₂ and Ti₂Al₅ was observed. It implies that the application of pulsed DC in our study did not alter the sequence of phase transformations for Ti/Al system. In a related study on field-activated combustion synthesis of titanium aluminides, the formation of each intermetallic compound under self-propagating combustion mode had a threshold value of imposed electric field for wave initiation and propagation.^[41] They are 14.3 V/cm² and larger than 15.7 V/cm² for the formation of Ti₃Al and TiAl, respectively. In our study, due to the nature of SPS technique, *i.e.*, high current and low voltage during sintering, the electric field imposed is about 1.5 V/cm² in our experiments, and hence, it is deemed highly unlikely that the electric field had any significant effect on the sequence of phase transformations. However, the reactions between Ti, Al, and their intermetallics exhibit enhanced kinetics during both the stages of sintering, which is reflected in the fact that the complete consolidation and the synthesis of γ -TiAl was attained with the two-step sintering within a few minutes. The high volume fraction of grain boundaries^[42], and the high densities of vacancies and dislocations^[43,44] which were generated by the large strains present during milling and the presence of electric field are all factors that are likely to have contributed to the enhanced reaction kinetics. A detailed study of the effect of these factors individually as well as in combination is presented in Part 2 of the current study.

V. SUMMARY

Fully lamellar γ -TiAl was processed by a rapid, two-stage, solid-state reactive sintering *via* spark plasma sintering (SPS) of a cryomilled Ti, Al powder blend. To provide insight into the concurrent influences of an electric field and a nanograined microstructure on the kinetics of diffusion, cryomilling was implemented in the current study to attain a nanostructured grain size in the Ti and Al powder blend.

1. After 10-hour cryomilling for the pure Ti and pure Al powder blend, the grain sizes of Ti and Al were refined to 100 and 42 nm, respectively.
2. The diffusion distance in the Ti and Al powders required for sintering and homogenization was reduced by the significant refinement of the particle size of Al powder.
3. By SPS cryomilled Ti and Al powder blend at 873 K (600 °C) for 15 minutes and 1523 K (1250 °C) for 30 minutes, γ -TiAl alloy can be prepared rapidly *via* solid-state diffusion between Ti and Al.
4. The strain energy experienced by Al in the 10-hour-cryo milling experiment is almost twice as much as that corresponding to Ti. It led to different microstructure and defect evolution for Al and Ti during cryomilling.
5. The application of pulsed DC did not alter the sequence of phase transformations for nanograin Ti/Al system.

ACKNOWLEDGMENTS

The experimental support and advice provided by Ertorer Osman, Haiming Wen, Yizhang Zhou, and Baolong Zheng is greatly appreciated. The authors would like to thank the management of General Motors for supporting this research. E.J.L. would also like to thank the support from National Science Foundation with a grant number NSF DMR-1210437.

REFERENCES

1. Z.A. Munir, U. Anselmi-Tamburini, and M. Ohyanagi: *J. Mater. Sci.*, 2006, vol. 41, pp. 763–77.
2. J. Zhao, J.E. Garay, U. Anselmi-Tamburini, and Z.A. Munir: *J. Appl. Phys.*, 2007, vol. 102, p. 114902.
3. J.E. Garay, U. Anselmi-Tamburini, and Z.A. Munir: *Acta Mater.*, 2003, vol. 51, pp. 4487–95.
4. N. Bertolino, J. Garay, U. Anselmi-Tamburini, and Z.A. Munir: *Philos. Mag. B*, 2002, vol. 82, pp. 969–85.
5. J.R. Friedman, J.E. Garay, U. Anselmi-Tamburini, and Z.A. Munir: *Intermetallics*, 2004, vol. 12, pp. 589–97.
6. T. Kondo, M. Yasuhara, T. Kuramoto, Y. Kodera, M. Ohyanagi, and Z.A. Munir: *J. Mater. Sci.*, 2008, vol. 43, pp. 6400–05.
7. U. Anselmi-Tamburini, J.E. Garay, and Z.A. Munir: *Mater. Mater. Sci. Eng. A*, 2005, vol. 407, pp. 24–30.
8. T. Kondo, T. Kuramoto, Y. Kodera, M. Ohyanagi, and Z.A. Munir: *J. Ceram. Soc. Jpn.*, 2008, vol. 116, pp. 1187–92.
9. H. Clemens and H. Kestler: *Adv. Eng. Mater.*, 2000, vol. 2, pp. 551–70.
10. K. Gebauer: *Intermetallics*, 2006, vol. 14, pp. 355–60.
11. K. Liu, Y.C. Ma, M. Gao, G.B. Rao, Y.Y. Li, K. Wei, X.H. Wu, and M.H. Loretto: *Intermetallics*, 2005, vol. 13, pp. 925–28.
12. T. Tetsui: *Mater. Mater. Sci. Eng. A*, 2002, vol. 329, pp. 582–88.
13. G.P. Chaudhari and V.L. Acoff: *Intermetallics*, 2010, vol. 18, pp. 472–78.
14. Y.Y. Chen, H.B. Yu, D.L. Zhang, and L.H. Chai: *Mater. Mater. Sci. Eng. A*, 2009, vol. 525, pp. 166–73.
15. M.A. Lagos and I. Agote: *Intermetallics*, 2013, vol. 36, pp. 51–56.
16. O. Ertorer, T. Topping, Y. Li, W. Moss, and E.J. Lavernia: *Scripta Mater.*, 2009, vol. 60, pp. 586–89.
17. D.B. Witkin and E.J. Lavernia: *Prog. Mater. Sci.*, 2006, vol. 51, pp. 1–60.
18. N. Bertolino, M. Monagheddu, A. Tacca, P. Giuliani, C. Zanotti, and U.A. Tamburini: *Intermetallics*, 2003, vol. 11, pp. 41–49.
19. G.K. Williamson and W.H. Hall: *Acta Metall.*, 1953, vol. 1, pp. 22–31.
20. L. Balogh, T. Ungar, Y. Zhao, Y.T. Zhu, Z. Horita, C. Xu, and T.G. Langdon: *Acta Mater.*, 2008, vol. 56, pp. 809–20.
21. J. Schuster and M. Palm: *J. Phase Equilib. Diffus.*, 2006, vol. 27, pp. 255–77.
22. L. Xu, Y.Y. Cui, Y.L. Hao, and R. Yang: *Mater. Mater. Sci. Eng. A*, 2006, vol. 435, pp. 638–47.
23. W. Yao, A.P. Wu, G.S. Zou, and H.L. Ren: *Mater. Mater. Sci. Eng. A*, 2008, vol. 480, pp. 456–63.
24. K. Kulkarni, Y. Sun, A.K. Sachdev, and E.J. Lavernia: *Scripta Mater.*, 2013, vol. 68, pp. 841–44.
25. H.M. Wen, T.D. Topping, D. Isheim, D.N. Seidman, and E.J. Lavernia: *Acta Mater.*, 2013, vol. 61, pp. 2769–82.
26. E.J. Lavernia, B.Q. Han, and J.M. Schoenung: *Mater. Mater. Sci. Eng. A*, 2008, vol. 493, pp. 207–14.
27. J. Benjamin and T. Volin: *Metall. Trans. B*, 1974, vol. 5B, pp. 1929–34.
28. F.S. Sun, P. Rojas, A. Zuniga, and E.J. Lavernia: *Mater. Mater. Sci. Eng. A*, 2006, vol. 430, pp. 90–97.
29. C. Suryanarayana: *Prog. Mater. Sci.*, 2001, vol. 46, pp. 1–184.
30. F. Zhou, D. Witkin, S.R. Nutt, and E.J. Lavernia: *Mater. Mater. Sci. Eng. A*, 2004, vol. 375, pp. 917–21.
31. O. Ertorer, A. Zuniga, T. Topping, W. Moss, and E.J. Lavernia: *Metall. Mater. Trans. A*, 2009, vol. 40A, pp. 91–103.
32. C.C. Koch: *Nanostruct. Mater.*, 1993, vol. 2, pp. 109–29.
33. Y.J. Lin, B. Yao, Z.H. Zhang, Y. Li, Y. Sohn, J.M. Schoenung, and E.J. Lavernia: *Metall. Mater. Trans. A*, 2012, vol. 43A, pp. 4247–57.
34. D.R. Lide: *Handbook of Chemistry and Physics*, 84th ed., CRC Press, Boca Raton, 2003.
35. G. Welsch, R. Boyer, and E.W. Collings: *Materials Properties Handbook: Titanium Alloys*, ASM International, Materials Park, 1994.
36. C.C. Koch: *Nanostruct. Mater.*, 1997, vol. 9, pp. 13–22.
37. T. Voisin, L. Durand, N. Karnatak, S. Le Gallet, M. Thomas, Y. Le Berre, J.F. Castagne, and A. Couret: *J. Mater. Process. Technol.*, 2013, vol. 213, pp. 269–78.
38. Y. Sun, K. Kulkarni, A.K. Sachdev, and E.J. Lavernia: *Metall. Mater. Trans. A*, DOI:10.1007/s11661-014-2216-2.
39. J. Safarian and T.A. Engh: *Metall. Mater. Trans. A*, 2013, vol. 44A, pp. 747–53.
40. J.G. Luo and V.L. Acoff: *Mater. Mater. Sci. Eng. A*, 2004, vol. 379, pp. 164–72.
41. R. Orru, G. Cao, and Z.A. Munir: *Metall. Mater. Trans. A*, 1999, vol. 30A, pp. 1101–08.
42. Y. Mishin and C. Herzig: *Mater. Mater. Sci. Eng. A*, 1999, vol. 260, pp. 55–71.
43. L.C. Luther: *J. Chem. Phys.*, 1965, vol. 43, pp. 2213–18.
44. E.W. Elcock and C.W. McCombie: *Phys. Rev.*, 1958, vol. 109, pp. 605–06.